Study of Multilayer FEP Characteristics Using Second Harmonic Generation Measurement

Sung-Kun Park, Ming Lei[1)], Youngwoong Do, Dong-Hyun Kim, Jae-Hyun Kim, Hyungbok Choi[2)], Seung-Han Lee[2)], Kyung-do Kim, Heon-Joon Kim, Sung-Bo Hwang, Hoon-Sang Oh, Sung-Joo Hong and Kyung-Dong Yoo[3)]

SK hynix, Technology Development Group, Icheon-si, Gyeonggi-do, Korea
[1)] Femtometrix Inc., 2811 McGaw Ave., Irvine, California 92614, USA
[2)] Wonik-IPS Inc., Pyeongtaek-si, Gyeonggi-do, Korea
[3)] Hanyang University, Nanoscale Semiconductor Engineering, Seoul 133-791, Korea
E-mail : sungkun1.park@sk.com, mobile phone : 82-10-2740-7113

***Abstract*— Second harmonic generation (SHG) characteristics of single and multilayer field effect passivation (FEP) structure were investigated for CMOS image sensor application. By compensating the internal multiple reflection (IMR) effect on SHG intensity, the characteristics of single and multilayer FEP structures were compared under equivalent conditions. Finite-Difference Time-Domain simulation reveals that due to IMR effect, the intensity of multilayer structure was reduced to around 60 % than the single FEP layer regardless to thin film thickness and refractive index variation. The major IMR effect difference was caused from 390 nm outgoing SHG signal. Analysis of the time-dependent SHG intensity confirmed that the multilayer structure has a 2.7 times higher SHG intensity than the single layer structure. Also, the FEP layer is negatively charged from the initial state. In addition, when atomic layer deposition conditions were changed to control the Al_2O_3 composition ratio, the oxygen-rich growth condition shows higher SHG intensity than using oxygen deficient growth conditions.**

***Index Terms*— Field effect passivation, Second harmonic generation, CMOS image sensor, Multilayer, High-k dielectrics**

I. INTRODUCTION

The pixel size of commercial CMOS image sensor (CIS) products has been reduced to 0.9 μm following demand for high resolution CIS pixels [1, 2]. Pixel size reduction results in low sensitivity and higher crosstalk due to an increase in diffraction. Thus, backside illumination (BSI) technology for higher sensitivity, and backside deep trench isolation (B-DTI) technology for crosstalk reduction have been developed for pixels smaller than 1.4 μm [2, 3]. However, BSI and B-DTI methods cause Si surface damage through the back side CMP and plasma etching process, resulting in dark current increases [4, 5]. In the early stage of BSI process development, a laser anneal method was used to activate p-type doping of the extremely shallow backside Si surface while avoiding affecting photodiode profiles. However, this method cannot cure B-DTI process induced Si damage because the depth of B-DTI under the Si surface is around 1 μm.

To solve this problem, a field effect passivation (FEP) method was adopted to suppress dark current by accumulating holes on the backside Si surface using a negative fixed charge of a high-k material. However, a multilayer FEP structure was used in the actual CIS product, but until now there has not been enough research on the multilayer structure [6~8].

In this study, we analyzed characteristics of the FEP layer depending on multilayer structures using second harmonic generation (SHG) measurement. SHG can directly measure the electric field strength of the space charge region (SCR) without additional processes and can be used for investigation of FEP properties [9, 10]. However, due to internal multiple reflection (IMR) caused from refractive index difference of each film, it is difficult to directly compare single and multilayer structures. In this report, direct comparison between single and multilayer structures was possible by compensating the IMR effect of the multilayer film structure. In addition, the influences of ALD processing conditions were also investigated to understand negative fixed charge generation mechanism of FEP layer.

II. EXPERIMENT

The multilayer FEP structures were fabricated with combination of interface oxide, Al_2O_3 and ZrO_2. Using these film stacks allowed for comparison of the characteristics of single and multilayer structure. As an interface oxide, the native oxide is grown on Si from the ambient atmosphere, whereas the plasma oxide is formed by O_3 plasma treatment.

Al_2O_3 and ZrO_2 films were deposited using HyEta-ALO and HK equipments of Wonik-IPS at 320 ℃ and 300 ℃, respectively to minimize the influence of high temperature during FEP deposition. The FEP layer formation conditions used in this experiment are listed in Table I.

TABLE I. FIELD EFFECT PASSIVATION LAYER FORMATION CONDITIONS

	Interface Oxide	**Al_2O_3**	**ZrO_2**
Growth mode	Oxidation	ALD	ALD
Condition	Native /Plasma	120 rpm@O_3 120 g/cm^3 ~12 rpm@O_3 215 g/cm^3	30 rpm
Temperature	Room/400℃	320℃	300℃
Source	Ambient Oxygen /O_3 Plasma	TMA	Cp-Zr
Thickness	11~22 Å	55 Å	550 Å

SHG measurement was carried out using time-dependent (TD)-SHG measurement equipment by FemtoMetrix. Fig. 1 describes the schematic layout of the SHG measurement used in this experiment and the principle of the TD-SHG evaluation method. A 780 nm pulse laser was used as input light, and a 390 nm SHG signal was detected. As laser irradiation time increases, injected electrons are trapped on the oxide creating additional negative charges and resulting in higher internal *E*-field at SCR [10].

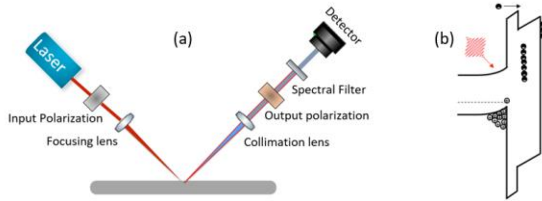

Fig. 1. (a) Schematic of SHG measurement system, (b) As laser irradiation time increases, injected electron will be trapped at oxide creating additional negative charges resulting in higher internal electric field at Si surface.

The SHG intensity for Si with a centrosymmetry structure is expressed as [10]

$$I^{(2\omega)}(t) \propto \left|\chi_{eff}^{(2)} + \chi_{eff}^{(3)} E_{DC}^{0}(t)\right|^2 \qquad (1).$$

Since E_{DC} is the *E*-field of SCR, the intensity of SHG is proportional to the internal *E*-field. We can therefore measure the internal *E*-field directly by measuring SHG intensity.

Fig. 1 (b) shows the electron injection mechanism by laser irradiation used in TD-SHG. We can evaluate the quality of the FEP layer by monitoring injected electron recombination characteristics, which can be quantified as the difference between final intensity and initial intensity (ΔSHG). We can also infer the direction of the initial internal *E*-field of SCR by monitoring the shape of the intensity increase during laser irradiation.

III. RESULTS AND DISCUSSION

A. IMR Characteristics of Multilayer Thin Film

In this experiment, the SHG characteristics of single or multilayer Al_2O_3 and ZrO_2 films were investigated. In the case of multilayer thin films, IMR may occur and influence transmission and reflection characteristics. Especially in the case of SHG measurement, two different wavelengths should be considered for IMR. In this experiment, an input wavelength of 780 nm and output wavelength of 390 nm were used for the Finite-Difference Time-Domain (FDTD) simulation to calculate the effect of IMR on SHG intensity.

Table II lists the refractive index of the FEP layers for two wavelengths. The order from smallest to largest refractive index for both 390 and 780 nm is SiO_2, Al_2O_3, ZrO_2, and Si.

TABLE II. REFRACTIVE INDEX OF MATERIALS

Wavelength	**Si**	**SiO_2**	**Al_2O_3**	**ZrO_2**
390 nm	5.94	1.47	1.79	2.23
780 nm	3.71	1.45	1.76	2.14

Fig. 2 shows the simulation conditions of the different stacked structures of the FEP layer and the normalized IMR intensity calculated by FDTD.

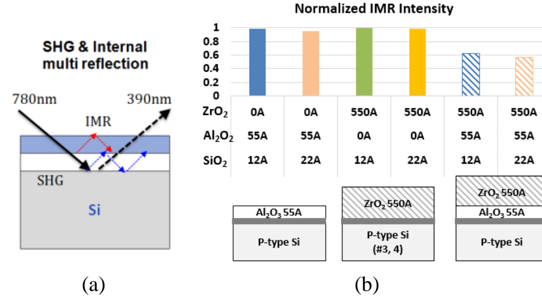

Fig. 2. (a) Schematic of IMR effect, (b) Normalized IMR effect of Finite-Difference Time-Domain (FDTD) simulation results by FEP film stack structure.

There is no significant difference in IMR characteristics for different SiO_2 thicknesses. Similarly, when using a single Al_2O_3/SiO_2 or ZrO_2/SiO_2 layer, there were no differences in intensity by IMR despite the large differences in refractive index and thickness. In contrast, when the multilayer ZrO_2/Al_2O_3/interface oxide was applied, the normalized output intensity was decreased by around 60 % due to IMR.

In this simulation, default refractive index of FDTD simulator and exact target film thicknesses were used.

However, in case of thin film, thickness variation can also affect IMR. Furthermore, refractive index of thin films depends on thickness and growth condition of film, results in different to FDTD simulator default value.

In Table III, we summarized previously published refractive index of SiO_2, Al_2O_3, ZrO_2 thin films [11, 12]. For example, ALD grown 100 Å thickness Al_2O_3, the refractive index for 390 nm and 780 nm are 1.686 and 1.66, respectively. However, for 55 Å and 1000 A thicknesses, the refractive indexes are 1.7 and 1.665 at 623.8 nm. Therefore, by using interpolation, we used refractive index of 1.721 and 1.695 at 390 nm and 780 nm respectively for 55 Å Al_2O_3. In case of ZrO_2,

thickness is relatively thick to 550 Å . Therefore, we use crystal structure value of 2.13 at 790 nm and 2.25 at 360 nm using same interpolation method.

TABLE III. REFRACTIVE INDEX OF THIN FILMS

Wavelength	SiO_2 (12 Å)	SiO_2 (22 Å)	Al_2O_3	ZrO_2
390 nm	2.04	1.96	1.721	2.25
780 nm	2.02	1.94	1.695	2.13

Fig. 3 displays IMR effect for ± 10 Å Al_2O_3 thickness variations and refractive index of each thin film. Regardless of film thickness or refractive index split, only multilayer FEP structure shows around 60 % decreased value of normalized intensity.

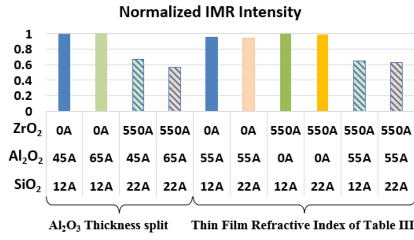

Fig. 3. Normalized IMR effect of FDTD simulation results depending on Al_2O_3 film thickness variation, and result of applying proper thin film refractive index listed in Table III.

Therefore, in this variation range, we can use default refractive index of FDTD simulator. By compensating for the SHG intensity, the influence of the IMR on SHG evaluation can be excluded making a direct comparison of pure internal *E*-field of SCR possible.

B. SHG Characteristics

Fig. 4 shows IMR compensated SHG intensity of single FEP layer with different interface oxide.

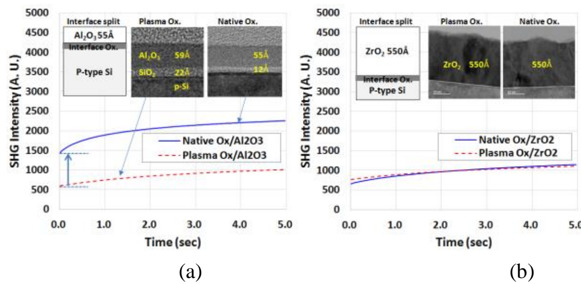

Fig. 4. SHG characteristics of a single FEP layer with respect to interface oxide. (a) Single Al_2O_3 layer, (b) Single ZrO_2 layer.

Compared to ZrO_2, the Al_2O_3 layer shows higher SHG intensity as expected in K. Kita's oxygen areal density mechanism [13]. In the case of ZrO_2, the SHG intensity is very low, and changing the interface oxide has no effect. In case of the Al_2O_3 layer, using the native oxide as an interface oxide results in higher SHG intensity than using the plasma oxide. This result is consistent with that of N. Terlinden the thickness of the native oxide is around 12 Å , whereas that of the plasma oxide is 22 Å [14]. As can be seen from the inset TEM images of Fig. 4, we can see the plasma oxide is 10 Å thicker than the native oxide. Also, in spite of the identical growth conditions, the Al_2O_3 that was grown on the plasma oxide layer was found to be around 4 Å thicker than that in the native oxide buffer case. However, as shown in Fig. 2 and Fig. 3, there was no big difference of IMR due to relatively thin layer thickness compared to SHG wavelength.

Furthermore, ΔSHG is smaller for the plasma oxide than for the native oxide, indicating higher recombination rate. The electrons, injected by laser irradiation, recombine with holes resulting in reduced increase of the internal *E*-field of SCR. This implies that plasma oxide has more trap density, which act as recombination centers.

Fig. 5 compares SHG characteristics of the multilayer FEP structure with respect to interface oxide. The $ZrO_2/Al_2O_3/SiO_2$ multilayer structure showed 2.7 times higher SHG intensity than the single layer structure, regardless of interface oxide.

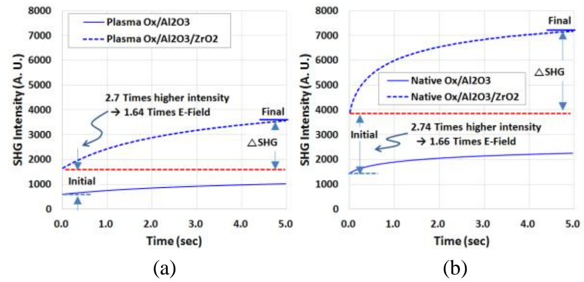

Fig. 5. SHG characteristics with respect to multilayer structure. (a) Plasma oxide interface layer, (b) Native oxide interface layer.

According to equation (1), 2.7 times higher SHG intensity indicates 1.64 times higher internal *E*-field. That means, the multilayer FEP layers has around 1.65 times higher internal *E*-field than single layer structures.

Fig. 6 presents SHG intensity and ΔSHG intensity with respect to the FEP layer structure. ΔSHG of multilayer FEP structures are also 3.1 to 3.5 times higher than the single FEP layer, implying a higher recombination blocking capability than for single layer structures.

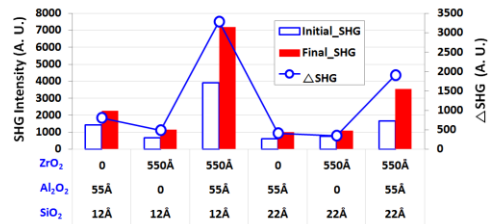

Fig. 6. Initial and final SHG intensity and ΔSHG intensity with respect to single and multilayer FEP structure. The multilayer FEP shows three times higher intensity than single layer structures.

According to K. Kita, the field effect passivation mechanism can be explained using the dipole formation model: displacement of oxygen is caused by the difference in oxygen areal density between two adjacent layers. H. Kamata also used this oxygen areal density model to explain the high V_{FB} shift of $Al_2O_3/SiO_2/Al_2O_3/SiO_2$ laminated dielectric films [15].

In this experiment, the SHG intensity of $ZrO_2/Al_2O_3/SiO_2$ is larger than that of a single FEP layer, implying the increase of total negative fixed charges, results in a larger internal *E*-field at SCR. That means the additional negative fixed charges are generated at the ZrO_2/Al_2O_3 interface besides to the Al_2O_3/SiO_2 or ZrO_2/SiO_2 interfaces.

To analyze the influence of oxygen areal density on a single layer, the effects of ALD growth conditions were examined. Fig. 7 compares the influence of SHG characteristics on the formation conditions of Al_2O_3.

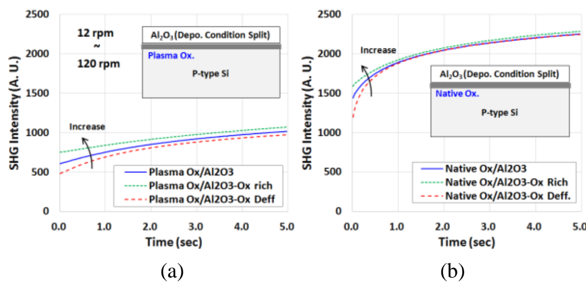

(a) (b)

Fig. 7. SHG characteristics with respect to Al_2O_3 growth condition using ALD. (a) Plasma oxide interface layer, (b) Native oxide interface layer.

The intensity of initial SHG increased with increasing ambient oxygen during film growth, implying that high levels of ambient oxygen can increase oxygen areal density and result in high negative fixed charges at the interface. However, when electrons were injected by laser pulse irradiation during TD-SHG measurement, the intensity was saturated in 5 s.

IV. Conclusion

In this experiment, we compared FEP characteristics of Al_2O_3/SiO_2, ZrO_2/SiO_2 and $ZrO_2/Al_2O_3/SiO_2$ structure by using SHG measurement. SHG can measure the *E*-field strength of the SCR without additional processes.

By compensating IMR effect which can occur in the multilayer thin film structure during SHG measurements, it was possible to evaluate different thicknesses and different stack structure films under equivalent conditions. For the film structures of this experiments, FDTD simulation reveals that the SHG intensity of multilayer ($ZrO_2/Al_2O_3/SiO_2$) structure was reduced to around 60 % of single FEP layer (Al_2O_3/SiO_2 and Al_2O_3/SiO_2) regardless to thin film thickness and refractive index variation. The major IMR effect difference was caused from 390 nm outgoing SHG signal.

The initial SHG intensity of multilayer FEP structure shows 2.7 times higher intensity than that of the single stack layer, implying a 1.64 times higher internal *E*-field at SCR. The results suggest that additional negative fixed charge can be generated at the ZrO_2/Al_2O_3 interface besides to the Al_2O_3/SiO_2 interfaces. In addition, the Al_2O_3 film grown in the oxygen-rich condition by ALD shows higher initial SHG intensity than films in other conditions, regardless of the type of interface oxide.

References

[1] H. Tian *et al.*, “Architecture and development of next generation small BSI pixels,” IISW, pp. 1-4, 2013.

[2] S. G. Wuu *et al.*, “A leading-edge 0.9 µm pixel CIS technology with BSI,” IEDM, pp. 14.1.1-14.1.4, 2010.

[3] R. Fontaine, “A Review of the 1.4 µm Pixel Generation,” IISW, pp. R2, 2011.

[4] A. Tournier *et al.*, “Pixel-to-pixel isolation by deep trench technology: Application to CIS, IISW, pp. R5, 2011.

[5] J-P Carrère, *et al.*, “CMOS image sensor: process impact on dark current,” IEEE IRPS, pp. 3C.1.1-3C.1.6, 2014.

[6] B. Hoex *et al.*, “Excellent passivation of highly doped p-type Si surfaces by the negative-charge dielectric Al_2O_3,” Appl. Phys. Lett., pp. 112107, 2007.

[7] D. K. Simon *et al.*, “On the control of the fixed charge densities in Al_2O_3-based silicon surface passivation schemes,” ACS Appl. Mater. Interfaces, pp. 28215–28222, 2015.

[8] P. M. Jordan *et al.*, “Trapped charge densities in Al_2O_3-based silicon surface passivation,” J. Appl. Phys., pp. 215306, 2016.

[9] J. Fiore *et al.*, “SHG probing of dopant type and density at the Interface,” Appl. Phys. Lett., pp. 041905, 2011.

[10] M. Lei *et al.*, “Detection of thermal donors from electrically active oxygen interstitials by SHG,” ASMC, pp. 197-201, 2018.

[11] C. Barbos *et al.*, “Al_2O_3 thin films deposited by thermal atomic layer deposition,” Thin Solid Films, pp. 108-113, 2016.

[12] Y. Wang and E. Irene, “Consistent refractive index parameters for ultrathin films,” J. Vac. Sci. Technol., pp. 279-282, 2000.

[13] K. Kita and A. Toriumi, “Origin of electric dipoles formed at high-k/SiO_2 interface,” Appl. Phys. Lett., pp. 13290021, 2009.

[14] N.M. Terlinden et al., “Influence of the SiO_2 interlayer thickness on the density and polarity of charges in $Si/SiO_2/Al_2O_3$ stacks as studied by optical SHG,” J. Appl. Phys., pp. 3033708, 2014.

[15] H. Kamata and K. Kita, “Design of Al_2O_3/SiO_2 laminated stacks with multiple interface dipole layers to achieve large flatband voltage shifts of MOS capacitors,” *Appl. Phys. Lett*., pp. 102106, 2017.